ISSN 0031-918X, The Physics of Metals and Metallography, 2015, Vol. 116, No. 5, pp. 467–474. © Pleiades Publishing, Ltd., 2015.
Original Russian Text © N.A. Krapivka, S.A. Firstov, M.V. Karpets, A.N. Myslivchenko, V.F. Gorban', 2015, published in Fizika Metallov i Metallovedenie, 2015, Vol. 116, No. 5, pp. 496–504.

STRUCTURE, PHASE TRANSFORMATIONS, AND DIFFUSION

Features of Phase and Structure Formation in High-Entropy Alloys of the AlCrFeCoNiCu$_x$ System (x = 0, 0.5, 1.0, 2.0, 3.0)

N. A. Krapivka[a], S. A. Firstov[a], M. V. Karpets[a], A. N. Myslivchenko[b], and V. F. Gorban'[a]

[a] *Institute of Materials Science Problems, National Academy of Sciences of Ukraine, ul. Krzhizhanovskogo 3, Kiev, 03680 Ukraine*

[b] *National Technical University of Ukraine Kiev Polytechnic Institute, pr. Pobedy 37, Kiev, 03056 Ukraine*

e-mail: zvyagina-47@yandex.ru

Received June 25, 2014; in final form, August 11, 2014

Abstract—Alloys of the AlCrFeCoNiCu$_x$ system (x = 0, 0.5, 1.0, 2.0, 3.0) were smelted by argon-arc smelting in pure argon. The phase composition and structure of fabricated alloys are investigated and their mechanical properties are determined. The results showed that an increase in the amount of copper in alloys leads to a change in the phase composition from single phase (bcc) to three phase (bcc + fcc$_1$ + fcc$_2$), which is accompanied by the structural change from coarse-grain polygonal structure to complex dendritic structure (primary dendrites (DR) + secondary dendrites (SDR) + interdendrite phase (ID)). The region of electron concentrations of alloys, in which bcc and fcc phases are present simultaneously, is determined. The limiting electron concentration of stability of the bcc lattice is found experimentally. Microhardness is measured and Young moduli of alloys over the entire range of varying the copper concentration are determined.

Keywords: high-entropy alloys, microstructure, crystallization, properties, phase formation

DOI: 10.1134/S0031918X15030084

INTRODUCTION

Ten years ago, J.W. Yeh developed scientific foundations and formulated formal criteria of material belonging to a new class of alloys that were called high-entropy equiatomic alloys (HEAs) [1]. According to these criteria, HEAs are alloys that contain no less than five elements. The content of each element should not exceed 35 at % and should not be lower than 5 at %. Classical examples of HEAs include multicomponent alloys, in which elements are present in equal atomic fractions.

This class of alloys is indeed new since the processes of structure and phase formation in them, as well as the diffusion mobility of atoms, mechanism of the formation of mechanical properties, and thermal stability differ substantially from similar processes in traditional alloys. The latter include the alloys that contain base elements (Fe, Ni, Mo, Al, etc.) that determine the crystal lattice of the material. The phase composition of such alloys can be easily predicted starting from binary or ternary phase diagrams, while the introduction of alloying additives leads either to the solid-solution strengthening of the initial lattice or the precipitation of dispersed phases.

Despite a large number of elements in HEAs, they most often crystallize in the form of simple bcc, fcc, and hcp solid solutions, and no precipitation of dispersed intermetallic compounds is observed in them [2]. This character of phase formation in HEAs is determined by a high entropy of mixing ($S_{mix} > 11$ J/(mol K)); therefore, the formation of low-entropy phases during crystallization from the melt occurs with a low probability. Currently, more than 100 various HEAs have been investigated. Despite that the investigations still have a purely scientific character, being still focused on establishing the regularities of the influence of various factors, including atomic size, electronegativity, enthalpy of mixing, electron concentration, etc., on the properties of formed HEAs [3], among the studied alloys there are materials that are already competitive with best traditional special alloys regarding hardness, heat resistance, fire resistance, corrosion resistance, wear resistance, and thermal stability.

As for the influence of the previously listed factors on phase formation in HEAs, only the relationship between the average electron concentration of alloy ρ and the type of the crystal lattice of the forming solid solution has been reliably established [4–5]; i.e., the hcp lattice is formed at ρ < 4.25 el/atom, the bcc lattice is formed in a range from 4.25 to 7.2 el/atom, and the fcc lattice is formed at ρ > 8.2 el/atom. A mixture of bcc and fcc solid solutions is formed in alloys with an electron concentration from 7.2 to 8.2 el/atom. In fact, the se concentration boundaries can shift depending on the crystallization rate of alloys and, therefore, the results of various authors for various alloys can be different [6]. From the viewpoint of practical application, the two-phase alloys that are formed

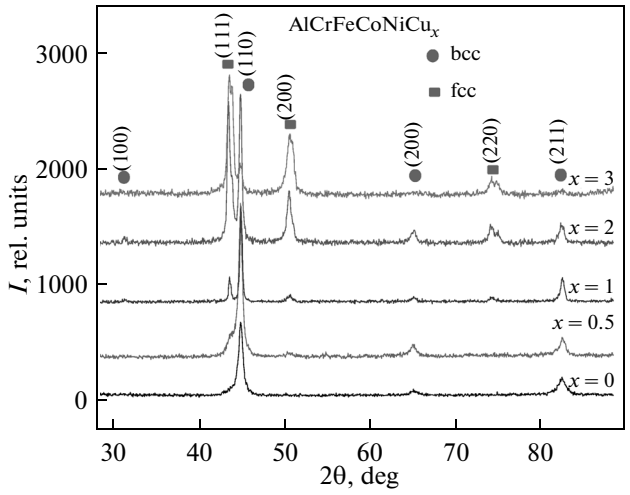

Fig. 1. X-ray diffractometry analysis of AlCrFeCoNiCu$_x$ system depending on the copper content.

as a result of joint crystallization of bcc and fcc phases are of most interest, since they represent a natural composite, in which branched bcc dendrites are the strengthening phase, while the interdendrite fcc solid solution is a plastic matrix. Varying the average electron concentration of the alloy in the coexistence range of two phases, we can control their volume ratio and, consequently, the strength and plastic properties of the material within wide limits.

We took the AlCrFeCoNi alloy, which is single-phase (bcc) and has already been studied rather well [7], as the initial HEA. We took copper as the sixth element for varying the electron concentration of the alloy for the following four reasons:

(1) each copper atom introduces maximum amount of electrons (eleven) into the system, which allows us to vary the average electron concentration in wide limits;

(2) copper has positive enthalpies of mixing with all elements except for Al and should fulfill the functions of a strongly segregating element during the crystallization;

(3) the atomic size of copper is very close to atomic sizes of Cr, Fe, Co, and Ni, which excludes the influence of the additional factor—dimensional mismatch—on the properties of the alloy;

(4) copper is situated in the same period as other elements of the alloy, which prevents an energy imbalance when combining the electrons in the alloy.

Investigations were aimed at establishing the regularities of the influence of copper on the phase and structure formation in AlCrFeCoNiCu$_x$ alloys ($x = 0$, 0.5, 1.0, 1.0, 3.0), as well as on their physicomechanical properties.

EXPERIMENTAL

Multicomponent AlCrFeCoNiCu$_x$ alloys were prepared in a MIFI-9 vacuum-arc furnace with an nonconsumable tungsten electrode by remelting a charge of 50 g in weight on a copper water-cooled bottom in purified argon. Components with purity no worse than 99.5% were used as the starting materials. Ingots were remelted six to seven times to homogenize the composition. Fragments weighing 7 g were melted out from the ingots and crystallized in the form of disks, which provided a cooling rate of 80–100 K/s. The bottom part of the ingots, in which the maximum cooling rate is implemented and crystallization defects (shrinkage porosity) and crystallographic texture are absent, was used for the investigations.

X-ray diffraction studies were performed in Cu $K\alpha$ radiation using an Ultima IV diffractometer (Rigaku, Japan). X-ray diffraction patterns were recorded by stepped scanning in the range of angles $2\theta = 28°–88°$. Experimental results were processed using the Powdercell 2.4 program for the full-profile analysis of X-ray diffraction spectra from a mixture of polycrystalline phase components.

Alloy microstructure was investigated using Superprobe-733 (JEOL) and 106I Selmi scanning electron microscopes (SEM); the latter is equipped with an energy dispersive analysis system (EDS), which allowed us to perform a local chemical analysis in the range of atomic numbers of elements from 11 (Na) to 92 (U) with a locality of 1 μm.

The physicomechanical characteristics of alloys were investigated by the microindentation method using a Micron-Gamma installation [8] under a load of up to $F = 0.3$ N with a diamond Berkovich tip with an angle of 65°, and loading and unloading automatically performed for 30 s. Diagrams of loading, holding, and unloading were recorded simultaneously in coordinates F–h. The accuracy of determining force F was 10^{-3} N and that of determining the indenter penetration depth h was ±2.5 nm. Characteristics of the diagram F, h_{max}, h_{res}, h_c, h_s were fixed using the data of 2000 points in the indentation diagram. In addition, characteristics of the material, such as hardness (H) and contact elasticity modulus (E_r) were automatically calculated according to the ISO 14577-1:2002(E) international standard.

RESULTS AND DISCUSSION

Phase Composition

Figure 1 shows X-ray diffraction patterns recorded for AlCrFeCoNiCu$_x$ alloys. It can be seen that, despite that the alloys include six elements, they crystallize as simple solid solutions with bcc and fcc lattices.

The initial AlCrFeCoNi alloy crystallizes in the form of a single-phase disordered bcc solid solution with lattice parameter 0.2884 nm. As the copper concentration in the melt increases, an fcc phase ($x = 0.5$,

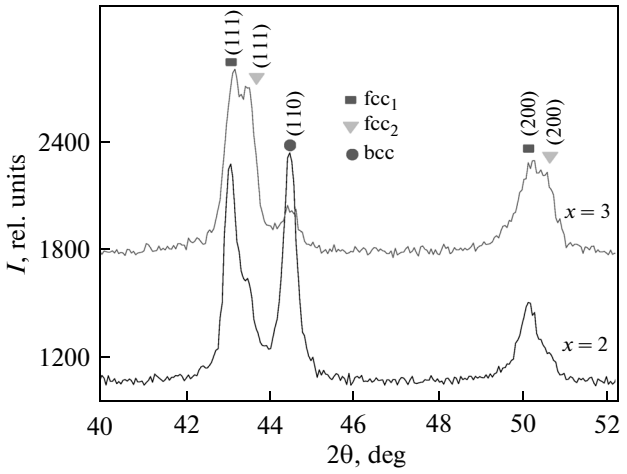

Fig. 2. Fragments of X-ray diffraction patterns of $AlCrFeCoNiCu_2$2 and $AlCrFeCoNiCu_3$ alloys.

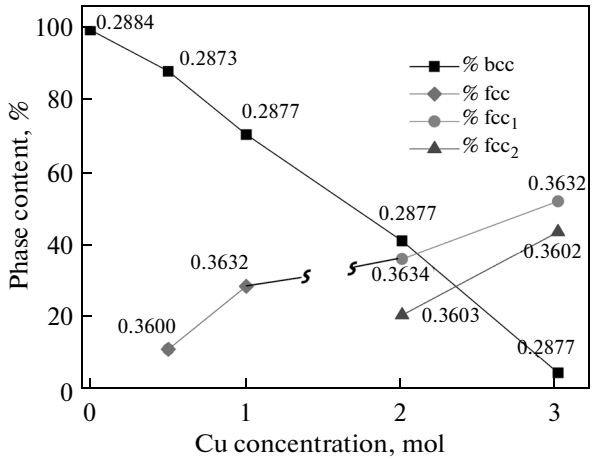

Fig. 3. Variations in the weight ratio between the phases depending on the copper content in $AlCrFeCoNiCu_x$ alloys. Lattice parameters of solid solutions (nm) are denoted above the points.

1.0) appears along with the bcc phase, and one more fcc_2 phase is precipitated at $x = 2$ and $x = 3$. Thus, over the entire concentration range of variations in the copper content, the number of phases varies from one (bcc) to three (bcc + fcc_1 + fcc_2). Figure 2 shows increased diffraction peaks for $AlCrFeCoNiCu_2$ and $AlCrFeCoNiCu_3$ alloys in the angle range $2\theta = 40°–52°$.

It can be seen that phases fcc_1 and fcc_2 only differ from one another by a small distinction in lattice parameters 0.3634 and 0.3603 nm, and the clear separation of these peaks is only possible at large angles ($2\theta > 70°$). The kinetics of varying the volume ratio between the phases is shown in Fig. 3.

It can be seen that, as the copper content varies from $x = 0$ to $x = 3.0$, the amount of the bcc phase decreases from 100 to 5%, and we can assume that, at a higher copper concentration, the alloy will be two-phase with (fcc_1 + fcc_2) lattices. It should be also noted that, in all of the studied alloys, the lattice parameter of the bcc phase varies insignificantly, just as the lattice parameters of the fcc_1 and fcc_2 lattices.

Structure

Like the phase composition, the structure of alloys is subjected to substantial changes as the amount of copper increases. The initial AlCrFeCoNi alloy crystallizes into the normal polygonal structure with grain size $d \approx 0.32$ mm and manifests no traces of a dendritic character of crystallization (Fig. 4a). The character of crystallization does not change at $x = 0.5$ except for the fact that the grain size substantially decreases ($d \approx$ 0.03 mm), while the grain boundaries are decorated by a thin interlayer of the fcc phase (Fig. 4b). The character of the structure formation changes at $x = 1.0$ (Fig. 4c); the dendritic character of crystallization of the bcc phase (DR) with traces of fragments of the segregating fcc phase between the branches of the growing dendrite (white points inside the dendrite body) are clearly distinguishable. The interdendrite space crystallizes in the form of the fcc phase (ID), and its amount increases. At copper content $x = 2.0$, the bcc phase crystallizes first in the form of well-branched dendrite as before (Fig. 4d, dark DR fragments). The structure of the interdendrite space becomes more complex. The larger part of this space is filled with well-branched gray dendrites SDR (fcc_1), which can be called secondary. The residual fcc_2 phase crystallizes in the space between the primary and secondary dendrites (Fig. 4d, bright ID phase). The character of crystallization does not change significantly at $x = 3.0$, but the contrast between the fcc_1 and fcc_2 phases becomes hardly distinguishable (Fig. 4e).

Mechanical Properties

Figure 5 shows experimental values of microhardness (H) and Young modulus (E) for all studied alloys over the entire range of variations in the copper concentration. The variations in microhardness are not monotonic, exhibiting a peak at $x = 0.5$, while the Young modulus decreases continuously as the copper content increases. Microhardness remains rather high for all alloys (from 3.4 to 6.1 GPa), while the Young modulus is rather low, especially when compared with the theoretical values calculated by the additivity law (the difference almost twofold) (Fig. 5).

DISCUSSION

The presented results show that the variations in the copper concentration in $AlCrFeCoNiCu_x$ alloys lead to both variations in the phase composition of alloys and variations in their structure and mechanical properties. The large degree of influence is probably

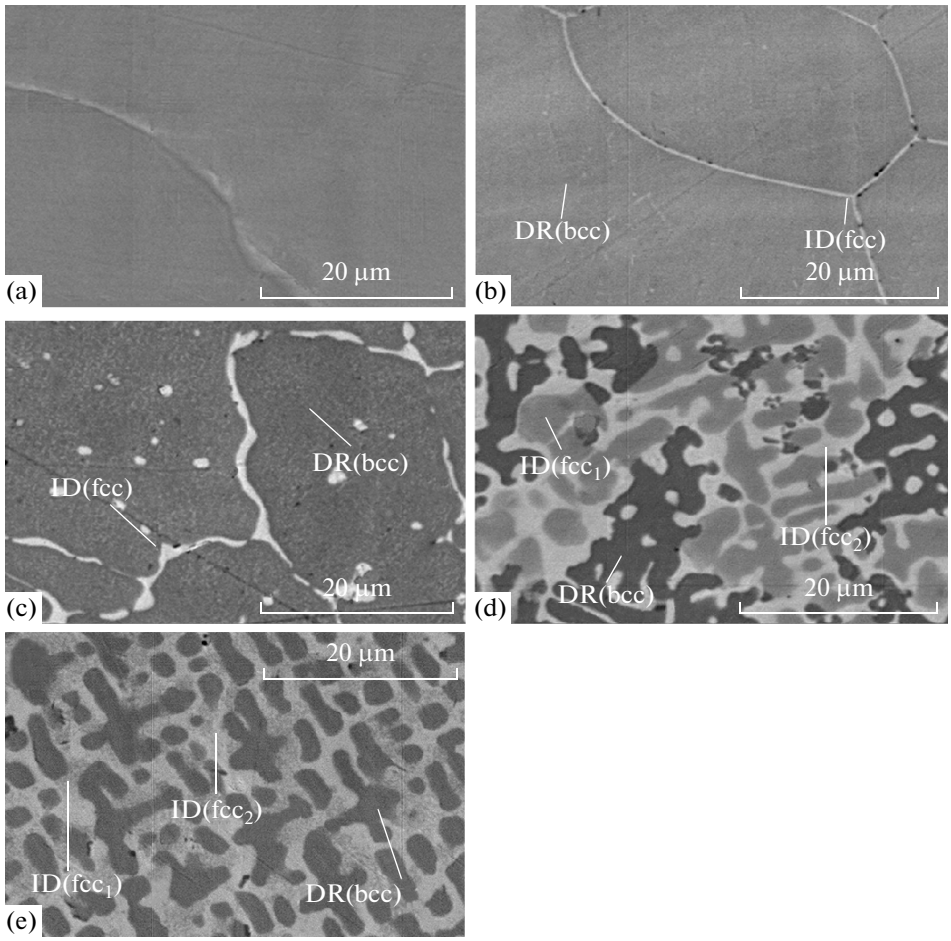

Fig. 4. Scanning electron microscopy images of the $AlCrFeCoNiCu_x$ alloy: (a) $x = 0$, (b) $x = 0.05$, (c) $x = 1.0$, (d) $x = 2.0$, and (e) $x = 3.0$.

because copper has a positive enthalpy of mixing with all elements of the alloy Cu–Fe, Cu–Cr, Cu–Co, and Cu–Ni except for Al (Table 1). It is thermodynamically unfavorable for copper atoms to be situated in the same lattice as these elements; therefore, it should be rejected by the crystallization front, i.e., it should segregate.

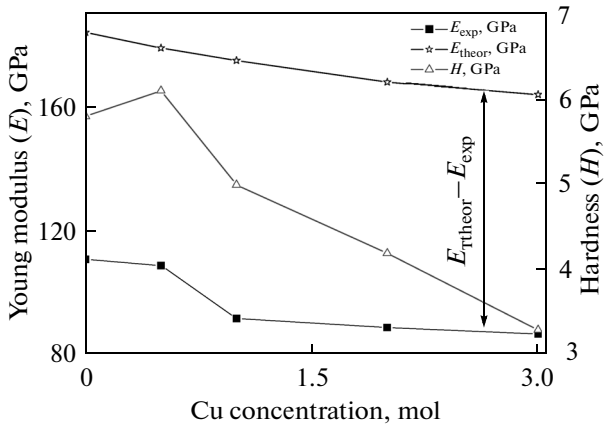

Fig. 5. Concentration dependence of microhardness and Young modulus for $AlCrFeCoNiCu_x$ alloys.

On the other hand, copper atoms increase the entropy of the alloy and, consequently, decrease its free energy and should partially enter the lattice. This compromise between a decrease in the internal energy of the crystallizing phase and an increase in the entropy leads copper to enter the bcc solid solution in a rather large amount of ~9 at % (Table 2).

Here, the size of copper atoms hardly differs from the size of other atoms (except for Al), which excludes the segregation due to the size discrepancy, and is a positive factor for the dissolution of copper. A similar system was investigated in [10], where copper was added by its analog silver, that has even larger enthalpies of mixing and a very unfavorable size factor. In this system, segregation leads to the complete separation of the alloy into pure silver and high-entropy alloy (silver hardly enters alloy lattice). Therefore, it is the behavior of copper during the alloy crystallization that mainly determines its phase and structural state.

Table 1. Enthalpies of mixing for atomic pairs with each element of the $AlCrFeCoNiCu_x$ alloy (kJ/mol) [9]

	Al	Cr	Fe	Co	Ni	Cu
Al	0	−10	−11	−19	−22	−1
Cr	−10	0	−1	−4	−7	+12
Fe	−11	−1	0	−1	−2	+13
Co	−19	−4	−1	0	0	+6
Ni	−22	−7	−2	0	0	+4
Cu	−1	+12	+13	+6	+4	0

No noticeable segregation occurs in the initial AlCrFeCoNi alloy with nonzero or negative enthalpies of mixing of all elements, and the alloy has a usual polygonal structure. The low copper concentration in the $AlCrFeCoNiCu_{0.5}$ alloy does not vary the character of crystallization, but leads to the appearance of the fcc phase (Fig. 4b). The analysis of the chemical composition of the grain and intergranular interlayer shows that copper hardly segregates at this concentration and its content in the grain body is even higher than in the intergranular interlayer (Table 2). There is also no large difference in the concentration of other elements in these phase regions; nevertheless, these regions crystallize into various lattices (Fig. 6). It can be seen from Fig. 6 that neither copper nor chromium in the alloy actually segregate.

The calculation of the average electron concentrations in these phases showed a small difference in their values (7.55 and 7.61 el/atom). It is probable that an electron concentration of 7.55 el/atom is the boundary at which the bcc lattice is still stable. It is probably appropriate to compare the reduced electron concentration with the electron concentration for pure metals at which the bcc lattice is stable. It is undoubtedly stable at electron concentrations of 5 el/atom (V, Nb, Ta) and 6 el/atom (Cr, Mo, W). At $\rho = 7$ el/atom, Mn has three allotropic modifications based on a cubic lattice, while Tc and Re have hexagonal lattices. Therefore, the question of stability of the bcc lattice at electron concentration $\rho > 6$ el/atom remains open both for pure elements and alloys.

The ability to achieve any electron concentration in the crystallizing phase and, thus, determine the boundary between the bcc and fcc lattices more precisely based on the electron concentration is a significant advantage of high-entropy alloys. The analysis of the results found based on the $AlCrFeCoNiCu_{0.5}$ alloy allows us to affirm that a concentration of 7.55 el/atom is the boundary of the bcc lattice existence at least for this set of elements and selected crystallization rate. Copper already noticeably segregates in the equiatomic alloy, in which the copper concentration exceeds its solubility in the bcc phase (~9 at %), and its concentration in the interdendrite fcc phase is 50 at %, which leads to the appearance of a clearly pronounced dendritic character of the crystallization of the bcc phase (Fig. 4c).

Excess undissolved copper in the $AlCrFeCoNiCu_{2.0}$ alloy leads to the formation of three solid solutions (Fig. 4d), and primary bcc dendrites have a close composition and the same lattice parameter as in alloys with $x = 0.5$ and 1.0. The segregating copper also governs the redistribution of other ele-

Table 2. Chemical composition (at %) of the system of cast $AlCrFeCoNiCu_x$ HEA

Alloy		Al	Co	Cr	Cu	Fe	Ni	r, el/atom	S_{mix} J (mol K)$^{-1}$
AlCrCoFeNi	Rated composition	20	20	20	0	20	20	7.2	13.3
$AlCrCoFeNiCu_{0.5}$	Rated composition	18.2	18.2	18.2	9	18.2	18.2	7.54	14.6
	Grain, DR	17.7	19	17.5	9.3	18	18	7.55	14.67
	Intergranular region, ID	17.6	20.3	16.1	8.4	19.6	18	7.61	14.62
AlCrCoFeNiCu	Rated composition	16.7	16.7	16.7	16.7	16.7	16.7	7.83	14.9
	Dendrite, DR	15	20	25	7	21	12	7.40	14.3
	Interdendrite region, ID	14	9	7	50	8	12	8.99	12.3
$AlCrCoFeNiCu_2$	Rated composition	14.3	14.3	14.3	28.6	14.3	14.3	8.28	14.53
	Dendrite, DR	18	19.4	19.9	11	16.3	15.4	7.50	14.72
	Secondary dendrite, SDR (fcc_1)	11	21.5	19	15	18.5	15	8.03	10.48
	Interdendrite region, ID (fcc_2)	11	8.2	6.6	55.7	7.5	11.5	9.34	11.58
$AlCrCoFeNiCu_3$	Rated composition	12.5	12.5	12.5	37.5	12.5	12.5	8.64	13.85
	Dendrite, DR	8.5	23	23	12	20	13.5	7.97	14.38

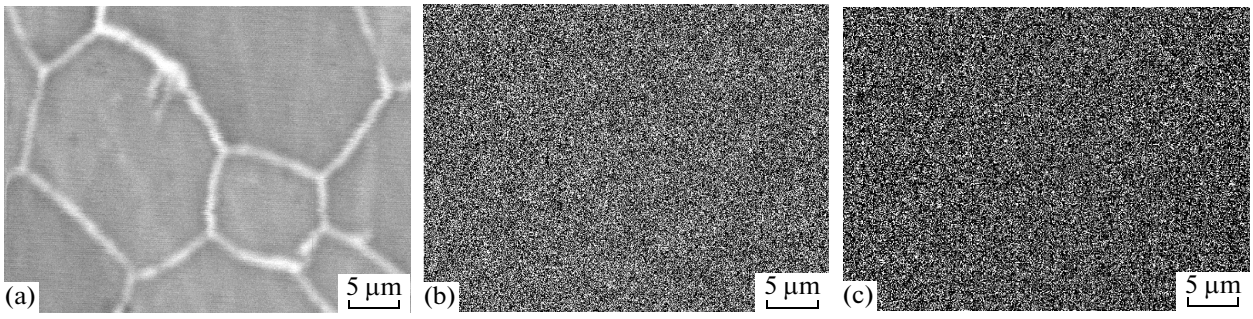

Fig. 6. Distribution of elements over the plane of the $AlCrFeCoNiCu_{0.5}$ sample in (a) backscattered electrons, (b) Cr $K\alpha$ radiation, and (c) Cu $K\alpha$ radiation.

ments, due to which the sequence of phase formation is as follows. As the primary bcc dendrites grow, the excess copper is collected before the crystallization front in the form of a thin interlayer that limits the diffusion exchange between the growing dendrite and host alloy. The presence of diffusion limitation at the crystallization front forces the dendrite to branch in the upper part, while the growth is retarded in the lower part because of the weak inflow of elements that would support the lattice parameter of the growing dendrite. As a result, the copper-enriched interdendrite melt starts to crystallize independently, and a new type of the lattice of new crystallization centers is determined by the electron concentration of the interdendrite liquid, which differs from the initial melt in the composition. In this case, the interdendrite melt has electron concentration $\rho > 7.55$ el/atom, since it is enriched with copper and crystallizes in the fcc lattice (SDR). Other elements that appeared at the lower concentrations in the crystallizing melt are present in the fcc phase in a considerable amount despite positive heats of mixing with copper (Cr, Fe, Co, Ni) (Table 2). The presence of segregating elements leads to the instability of the crystallization front, which results in a dendritic character (SDR) of crystallization of both the fcc and bcc phases, while the melt rejected by the crystallization front crystallizes as an independent third ID phase (the fcc_2 solid solution). This sequence of crystallization processes leads to the observed structural state of the alloy (Fig. 4d).

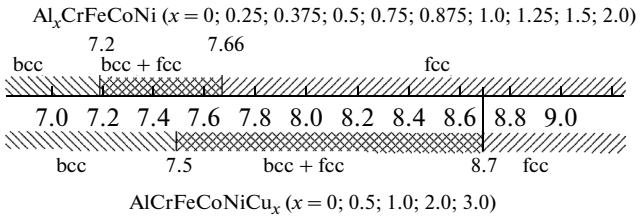

Fig. 7. Coexistence ranges of bcc and fcc phases depending on the average electron concentration for AlCrFeCoNi and $AlCrFeCoNiCu_x$ alloys.

The higher copper concentration in the $AlCrFeCoNiCu_3$ alloy leads to a further decrease in the amount of the bcc phase. The fact that the primary dendrite in this alloy, which is associated with the bcc phase, has an electron concentration calculated by a chemical composition of 7.97 el/atom, is associated with the specificity of a fine dendrite structure and the features of determining its chemical composition. The authors of [11, 12] showed that dendrites are not single-phase (bcc) but contain dispersed inclusions of the fcc phase. Since we perform the local chemical analysis from an area of ~1 μm^2, where bcc and fcc phases find themselves simultaneously, this integral analysis leads to an apparent increase in the amount of copper and electron concentration of the bcc phase. The chemical analysis with higher locality is necessary in these cases. The bulk fraction of the bcc phase visually seems to be higher than 5% by the same reason.

Processes of phase formation are more informative if we turn our attention from the copper concentration to the electron concentration of the melt from which the crystallization occurs (Fig. 7). Numerous articles [3, 4, 13] are devoted to the interrelation of the type of the alloy lattice and average electron concentration, and different regions of electrons concentrations are prescribed to the joint separation of (bcc + fcc) phases, notably, (6.89–8.0) el/atom in [13] and (7.2–8.2) el/atom in [3, 4]. It seems likely that this range is unique for each alloy depending on the element, as a result of which the electron concentration changes and its extension is determined by the degree of segregation of this element in this system. For copper, which can be considered a strongly segregating element because of the positive enthalpy of mixing, the coexistence range in our alloys is extended from 7.5 to 8.7 el/atom (Fig. 7). We plotted the results of investigations [14] for the $Al_xCrFeCoNi$ system, in which the electron concentration varied due to Al, on the same figure for comparison. From the viewpoint of enthalpies of mixing, Al is not a segregating element, although the segregation is possible from the viewpoint of the size factor. The coexistence range of (bcc + fcc) phases in this system turns out to be the narrowest among those previously presented in

publications (from 7.2 to 7.66 el/atom). It seems likely that if we additionally decrease the degree of segregation of elements in the alloy and narrow the crystallization range due to the selection of elements, the region of the coexistence of phases can be even narrower.

In general, the type of lattice of the crystallizing phase and its lattice parameter are formed during the formation of the crystallization nucleus from the high-entropy melt. The liquid–solid phase transition will occur as follows when the free energy in the Gibbs equation will be smaller than zero:

$$\Delta F = \Delta H - T\Delta S < 0.$$

ΔH and ΔS completely depend on what elements and in what amounts will participate in the formation of the crystallization nucleus. From the viewpoint of ΔH, the formation of a nucleus due to elements with negative enthalpies of mixing is more favorable energetically. Therefore, the elements with the positive enthalpy of mixing only enter the crystallization nuclei due to the entropy factor, and their concentrations in the nucleus can be considerably lower than in the melt. If these elements are principal electron donors ($\rho >$ 8 el/atom), the electron concentration in the crystallization nucleus can turn out to be considerably lower than in the melt, and if this concentration will be <7.55 el/atom, the nucleus will have the bcc DR lattice. As the nucleus grows, its lattice parameter remains invariable, while the electron concentration can vary right up to the limiting one for the bcc phase of 7.55 el/atom (Fig. 8). It can be seen that the electron concentration of the melt, which is the basic factor when developing the alloy composition, is not realized in any of crystallized phases (DR, SDR, and ID). If we speak about general regularities, then the concentration coexistence range of bcc and fcc phases is determined by the extent to which the elements with a high electron concentration participate in the formation of the crystallization nucleus, i.e., the lower their concentration in the nucleus, the more extended their range.

The bcc phase has the maximum hardness, and in a two-phase alloy the latter is proportional to the bulk fraction of the bcc phase. The regularities of varying the microhardness and Young modulus completely coincide with the character of varying the bulk ratio between the phases. The maximum microhardness at copper concentration $x = 0.5$ is apparently conditioned by the size factor, since, compared with the average grain size in the initial AlCrFeCoNi alloy, their sizes in the $AlCrFeCoNiCu_{0.5}$ alloy decrease more than tenfold, which leads to additional strengthening according to the Hall–Petch relation. Copper is a good modifier at this concentration. An increase in the copper concentration decreases both the theoretical Young modulus and the one determined experimentally. The fact that the actual modulus in each alloy is almost twofold smaller than the theoretical

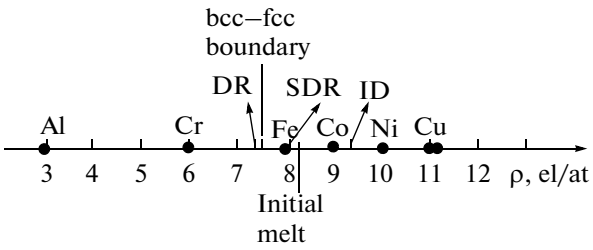

Fig. 8. Electron concentrations of phases in the $AlCrFeCoNiCu_2$ alloy.

value is associated with strong lattice distortion due to the size and elastic discrepancy of the atoms caused by the difference in interatomic interaction forces, as a result of which the atoms are shifted from lattice sites and maximum forces of the interatomic bond are not implemented.

It should be noted that plasticity at room temperature appears in alloys in the range of the copper concentration from $x = 1.0$ to $x = 2.0$ due to an increase in the amount of the fcc phase. A high plasticity (16%) is observed even for the equiatomic AlCrFeCoNiCu alloy during the compression test at room temperature, and it increases as the copper concentration increases. Microhardness of alloys remains at a sufficiently high level in this case. Due to the broad coexistence range of bcc and fcc phases, we can find such combination of elements in the $AlCrFeCoNiCu_x$ system of alloys that will provide a satisfactory ratio of strength and plasticity due to the favorable balance of phases.

CONCLUSIONS

(i) The phase composition in the alloys of the $AlCrFeCoNiCu_x$ system (x = 0, 0.5, 1.0, 2.0, 3.0) changes from a single-phase (bcc) to three-phase (bcc + fcc_1 + fcc_2) as the copper concentration increases, while the structure changes from simple coarse-grain polygonal to three-component one (primary bcc dendrite + secondary fcc_1 dendrite + fcc_2 interdendrite spacing). Lattice parameters of forming phases in various alloys have close values a_{bcc} = 0.2877 nm, $a_{fcc_1} = 0.3634$ nm, and $a_{fcc_2} = 0.3603$ nm. The sequence of phase formation depends on the degree of segregation of copper being determined by values of its enthalpies of mixing with other elements.

(ii) The stability boundary of the bcc lattice for these alloys and selected crystallization rate lies at the electron concentration $\rho \sim 7.55$ el/atom. It is noteworthy that the bcc and fcc phases coexist in a broad range of electron concentrations of alloys from 7.5 to 8.7 el/atom. The extension of the range is determined by the concentration of copper atoms and other elements with a high electron concentration in primary dendrites of the bcc phase. The lower their concentra-

tion, the wider the range of the joint crystallization of the bcc and fcc phases.

(iii) As the copper concentration in HEAs increases, microhardness decreases from 6.1 to 3.7 GPa and the Young modulus decreases from 112 to 85 GPa. This behavior is a reflection of the variations in the fraction of the bcc phase in alloys. High microhardness and low Young moduli are associated with lattice distortions caused by the size and elastic discrepancy of the atoms, which is caused by the difference in interatomic interaction forces. Satisfactory room-temperature plasticity appears in alloys in the range of copper concentrations from $x = 1.0$ to $x = 2.0$.

REFERENCES

1. J. W. Yeh, Y. L. Chen, and S. J. Lin, "High-entropy alloys—A new era of exploitation," Mater. Sci. Forum **560**, 1–9 (2007).
2. S. A. Firstov, V. F. Gorban', N. A. Krapivka, E. P. Pechkovskii, N. I. Danilenko, and M. V. Karpets, "Mechanical properties of cast multicomponent alloys at high temperatures," Sovrem. Probl. Fiz. Materialoved., No. 18, 140–147 (2009).
3. G. Sheng and C. T. Liu, "Phase stability in high entropy alloys: Formation of solid-solution phase or amorphous phase," Prog. Natur. Sci.: Mater. Intern., **21**, 433–446 (2011).
4. S. A. Firstov, V. F. Gorban', N. A. Krapivka, and E. P. Pechkovskii, "New class of materials—High-entropy alloys and coatings," Vestnik TGU, **18** (4), 1938–1940 (2013).
5. V. F. Gorban', V. A. Nazarenko, N. I. Danilenko, M. V. Karpets, N. A. Krapivka, S. A. Firstov, and E. S. Makarenko, "Effect of deformation on the structure and mechanical properties of the $Fe_{25}Cr_{20}Ni_{20}Co_{10}Mn_{15}Al_{10}$ high-entropy alloy," Deform. Razrush. Mater., No. 9, 2–6 (2013).
6. S. A. Firstov, T. G. Rogul', N. A. Krapivka, S. S. Ponomarev, V. V. Kovylyaev, N. D. Rudyk, V. Karpets, and A. N. Myslivchenko, "Effect of the rate of crystallization on the structure, phase composition, and strength of an AlTiVCrNbMo high-entropy alloy," Deform. Razrush. Mater., No. 10, 8–15 (2013).
7. Y. F. Kao, T. J. Chen, S. K. Chen, and J. W. Yeh, "Microstructure and mechanical property of as-cast, -homogenized, and -deformed $Al_xCoCrFeNi$ ($0 \le x \le 2$) high-entropy alloys," J. Alloys Compd., **488**, 57–64 (2009).
8. S. R. Ignatovich and I. M. Zakiev, "Universal nanohardness tester "Micron-Gamma"," Zavod. Lab. Diagn. Mater. **77** (1), 61–67 (2011).
9. A. Takeuchi and A. Inoue, "Classification of bulk metallic glasses by atomic size difference, heat of mixing and period of constituent elements and its application to characterization of the main alloying element," Mater. Trans. **46**, 2817–2829 (2005).
10. A. Munitz, M. J. Kaufman, J. P. Chandler, H. Kalaantari, and R. Abbaschian, "Melt separation phenomena in CoNiCuAlCr high-entropy alloy containing silver," Mater. Sci. Eng., A, **560**, 633–642 (2013).
11. O. N. Senkov, S. V. Senkova, C. Woodward, and D. B. Miracle, "Low-density, refractory multi-principal element alloys of the Cr–Nb–Ti–V–Zr system: Microstructure and phase analysis," Acta Mater. **61**, 1545–1557 (2013).
12. S. Singh, N. Wanderka, B. S. Murty, U. Glatzel, and V. J. Banhart, "Decomposition in multi-component AlCoCrCuFeNi high-entropy alloy," Acta Mater., **59**, 182–190 (2011).
13. G. Sheng, N. Chun, L. Jian, and C. T. Liu, "Effect of valence electron concentration on stability of fcc or bcc phase in high-entropy alloys," Appl. Phys., **109**, 103–109 (2011).
14. H. P. Chou, Y. S. Chang, S. K. Chen, and J. W. Yeh, "Microstructure, thermophysical and electrical properties in $Al_xCoCrFeNi$ ($0 \le x \le 2$) high-entropy alloys," Mater. Sci. Eng., B. **163**, 184–189 (2009).

Translated by N. Korovin